Comparison of ozone profiles from DIAL, MLS, and chemical transport model simulations over Río Gallegos, Argentina during the spring Antarctic vortex breakup, 2009

Takafumi Sugita[1], Hideharu Akiyoshi[1], Elián Wolfram[2], Jacobo Salvador[2,4,5], Hirofumi Ohyama[3,1], and Akira Mizuno[3]

[1]National Institute for Environmental Studies, Tsukuba, Ibaraki, Japan
[2]Laser Application Research Center (CEILAP)-UNIDEF (MINDEF-CONICET), UMI-IFAECI-CNRS-3351, Villa Martelli, Argentina
[3]Institute for Space-Earth Environmental Research (ISEE), Nagoya University, Nagoya, Aichi, Japan
[4]Universidad Tecnológica Nacional, Facultad Regional Bs. As. (UTN-FRBA) Medrano 951 CABA, Argentina
[5]Universidad Nacional de la Patagonia Austral Unidad Académica Río Gallegos and CIT Santa Cruz, Argentina

Correspondence to: T. Sugita (tsugita@nies.go.jp)

Abstract. This study evaluates the agreement between ozone profiles derived from the ground-based DIfferential Absorption Lidar (DIAL), satellite-borne Aura Microwave Limb Sounder (MLS), and 3-D chemical transport model simulations (MIROC-CTM) over the South Patagonian Atmospheric Observatory (OAPA, 51.6°S, 69.3°W) in Río Gallegos, Argentina from September to November 2009. In this austral spring, measurements were performed in the vicinity of the polar vortex, and inside it on some occasions; they revealed the variability in potential vorticity (PV) of measured air masses. Comparisons between DIAL and MLS were performed between 6 hPa and 100 hPa with 500 km and 24 h coincidence criteria. The results show a good agreement between DIAL and MLS with mean differences of ±0.1 ppmv (MLS – DIAL, n = 180) between 6 hPa and 56 hPa. MIROC-CTM also agrees to DIAL, with mean differences of ±0.3 ppmv (MIROC-CTM – DIAL, n = 23) between 10 hPa and 56 hPa. Both comparisons provide mean differences of 0.5 ppmv (MLS) to 0.8-0.9 ppmv (MIROC-CTM) at the 83-100 hPa levels. DIAL tends to underestimate ozone values at this lower altitude region. Between 6 hPa and 8 hPa, the MIROC-CTM ozone value is 0.4-0.6 ppmv (5-8%) smaller than those from DIAL. Applying the scaled PV criterion for matching pairs in the DIAL/MLS comparison, the variability in the difference decreases 21-47% between 10 hPa and 56 hPa. However, the mean differences are slight for all pressure levels, except 6 hPa. Because ground measurement sites in the Southern Hemisphere are very sparse at mid- to high-latitudes, i.e., 35-60°S, the OAPA site is unique for evaluating the bias and long-term stability of satellite instruments. The good performance of this DIAL system will be useful for such purposes in the future.

1 Introduction

Ozone depleting substances (ODS) have been decreasing since the Montreal Protocol and its subsequent adjustments and amendments. As a result, stratospheric ozone (O_3) is expected to increase in the future. The last WMO/UNEP ozone assessment concluded that increasing O_3 has been observed in the upper stratosphere around 42 km, or 2 hPa, in altitude (WMO, 2014).

5   Positive trends have been evaluated for both the tropics and 35-60° latitude bands of both hemispheres above 5 hPa levels from 2000 to 2016 (Steinbrecht et al., 2017). However, the trend is still not statistically significant below 10 hPa levels. Steinbrecht et al. (2017) found 0.7 ± 0.9 and $-0.2 \pm 1.4\%$ per decade changes at 10 hPa and 70 hPa, respectively, for 35-60°S. The satellite measurement has an advantage for estimating long-term trends because of its global coverage on a daily basis. However, its drift, i.e., the long-term measurement stability, should be quantitatively assessed with independent instruments. Ground-based

10 ozone lidar is a potential candidate for such purposes, and can be used to estimate drift (e.g., Nair et al., 2011, 2012; Eckert et al., 2014; Hubert et al., 2016).

Hubert et al. (2016) comprehensively evaluated the bias and drift of 14 limb-viewing satellite sensors using ozonesonde and ozone lidar measurements. They concluded that biases in the satellite sensors were within $\pm 5\%$ between 20 and 40 km and drifts were at most $\pm 5\%$ per decade. They suggested that several instruments have significant drifts; caution is needed for

15 multi-instrument comparisons to derive drift. Hubert et al. (2016) also showed a comparison spread, which is a measure of the short-term variability, with values of <5-12% for the same altitude range.

The ozone DIfferential Absorption Lidar (DIAL) system was installed at the South Patagonian Atmospheric Observatory (Observatorio Atmosférico de la Patagonia Austral, OAPA, 51.6°S, 69.3°W) in Río Gallegos, Argentina in 2005 (Wolfram et al., 2008). This site has been a stratospheric ozone lidar site within the Network for the Detection of Atmospheric Compo-

20 sitions Change, NDACC (www.ndsc.ncep.noaa.gov) since December 2008. NDACC sites in the Southern Hemisphere (S.H.) are very sparse at mid- to high-latitudes (e.g., 35-60°S). In springtime, this site is occasionally inside the southern polar vortex, which has shifted off the pole or elongated. A long persistent coverage (∼20 days) of the polar vortex over the southern tip of South America occurred in 2009 for the first time since 1979 (de Laat et al., 2010; Wolfram et al., 2012). In the 2009 austral spring between September and November, measurements at OAPA were performed in the vicinity or, on some occasions, in-

25 side of the polar vortex, revealing a variability in potential vorticity (PV) of measured air masses inside and outside the vortex. Accordingly, the largest variability in O_3 values would be expected in such a latitude band (35-60°S). Therefore, this event was a good opportunity to assess the impact of O_3 variability on biasing behavior. To evaluate the performance of the DIAL system under such variability, O_3 data from Aura Microwave Limb Sounder (MLS) satellite measurements (Waters et al., 2006) were used for comparison. In addition to the DIAL/MLS comparison, we also used O_3 values from a 3-D chemical transport model

30 simulation, which is based on version 3.2 of the Model for Interdisciplinary Research on Climate (MIROC) (Akiyoshi et al., 2016). Therefore, a secondary objective of this study was to examine the performance of the model simulation. Measurement and model simulation data used here are described in Section 2. The methodology used for the comparison is provided in Section 3. Vertical profiles of O_3 and their time series at the two selected pressure levels are shown in Section 4. The results of

differences that depend on coincidence criteria are also shown in Section 4 and summarized for all pressure levels (from 6 hPa
to 100 hPa). The conclusions of this study are described in Section 5.

2 Measurements and model simulations

2.1 Stratospheric ozone lidar

5 DIAL is a laser-based active remote sensing system operated from the ground, aircraft, and ship. O_3 measurements from DIAL
have a high vertical resolution and measurements have shown long-term stability (Nair et al., 2012; Hubert et al., 2016). To
target the stratosphere, O_3 number density is usually retrieved between 15 km and 45 km in geometric altitude. The DIAL
system installed at the OAPA site in Río Gallegos, Argentina, began operating in August 2005 (Wolfram et al., 2008). The
DIAL system operated at this site is fully described in Wolfram et al. (2008) and included in a review (Antuña-Marrero
10 et al., 2017). The instrument is briefly described here. The DIAL technique requires two emitted wavelengths generated by
two emitter lasers. An excimer (XeCl) laser emitting at 308 nm with 30 Hz repetition rate and maximum energy per pulse
of 300 mJ is used for ozone absorption. The reference wavelength corresponds to the third harmonic of the Nd-YAG laser
emission at 355 nm with 30 Hz repetition rate and maximum energy per pulse of 130 mJ. The optical receiver that collects
the backscattered photons is composed of four Newtonian (f/2) telescopes defining an array of telescopes. Each has a 50-cm
15 diameter with parabolic aluminized surfaces, 48-cm in diameter. This produces a total reception area of 7238 cm^2. An optical
fiber, 0.27 db km^{-1} with attenuation at 308 nm, is placed at the focus of each telescope. The other end of the fiber is positioned
at the focus of a quartz lens placed inside a spectrometer used to separate the received wavelengths. A mechanical chopper is
positioned at the entrance of the spectrometer. It has a rotational frequency of 300 Hz (18,000 rpm), and its role is to block the
strong lidar signals originating from the lower part of the atmosphere, typically below 10 km.
20   The O_3 number density profile is computed using the DIAL equation from the difference between the signal slopes origi-
nating from Rayleigh scattering of the emitted laser beams. Because lidar signals cover a large dynamic range, they have to
be attenuated for measurements in the lower stratosphere. Therefore, the final O_3 profile corresponds to a composite profile
computed from the "low" and "high" energy Rayleigh signals which are detected simultaneously (e.g., Godin et al., 1989).
      In the 2009 spring, measurements began on September 6 (UTC, Coordinated Universal Time) during clear-sky local night-
25 time. Because the latitude of OAPA is 51.6°S, the short night lengths with increased seasonal cloud cover made it challenging
to perform measurements after December (Wolfram et al., 2012). In total, 23 vertical profiles of ozone were obtained between
September and November 2009, which were used for this study. Most measurements were performed for 3-5 h to obtain a good
signal-to-noise ratio, leading to a horizontal spatial resolution of 300-500 km (assuming ~30 m/s wind speed). The actual
vertical resolution ranged from 0.7 km to 4 km at 14 km and 35 km in altitude, respectively. The total measurement uncertainty
30 also ranged from 3% to 15% at the same altitudes.

2.2 Aura MLS

The MLS measurement covers latitudes between 82°N and 82°S since August 2004 (Waters et al., 2006). It is onboard the National Aeronautics and Space Administration (NASA) Earth Observing System (EOS) Aura satellite. MLS measures millimeter- and submillimeter-wavelength thermal emission from the limb of the Earth's atmosphere every 25 seconds, from which vertical profiles of more than 15 chemical species are retrieved. We used the standard O_3 data product (240 GHz radiances) retrieved with the version 4.2 data processing algorithm, which is publicly available from mls.jpl.nasa.gov/. The quality of the O_3 data is as follows from Livesey et al. (2015). The vertical × horizontal resolutions are 3 km × 300 km at 100 hPa and 3 km × 500 km at 10 hPa. The precision is 0.03 ppmv at 100 hPa and 0.1 ppmv at 10 hPa. The accuracy estimated from systematic uncertainty characterization tests are 0.05 ppmv at 100 hPa and 0.3 ppmv at 10 hPa. Data screening was accomplished according to Livesey et al. (2015). The former versions of the MLS O_3 values are evaluated from comparisons with DIAL (Jiang et al., 2007). They showed a good agreement of ∼5% from 5 hPa to 100 hPa.

2.3 Nudged chemistry-climate model based on MIROC3.2 GCM

As described in Akiyoshi et al. (2016), NIES developed nudged chemistry-climate models (CCMs) using the MIROC model. The CCM was nudged toward European Center for Medium-Range Weather Forecasts (ERA)-Interim data below 1 hPa (Dee et al., 2011). In these nudged-CCMs, a set of model variables for zonal-wind (u), meridional wind velocities (v), and temperature (T) were nudged. Above 1 hPa, where no ERA-Interim pressure level data exist, the zonal-means of zonal wind and temperature are nudged toward the COSPAR international Reference Atmosphere 1986 data (CIRA, 1990). The time scale for nudging the meteorological data (u, v, and T) was set to one day.

The model used in this study is a spectral model with T42 horizontal resolution (2.8° × 2.8°) and 34 vertical atmospheric layers above the surface. The top layer is located at approximately 80 km (0.01 hPa). Hybrid sigma-pressure coordinates are used for the vertical direction. The chemical constituents included in this model are O_x, HO_x, NO_x, ClO_x, BrO_x, hydrocarbons for methane oxidation, heterogeneous reactions for sulfuric-acid aerosols, supercooled ternary solutions, nitric-acid trihydrate, and ice particles. The CCM contains 61 chemical constituents including 42 for prediction and 19 for photochemical equilibrium, 165 gas-phase reactions, 42 photolytic processes, and 13 heterogeneous reactions on multiple aerosol types. The reaction rates and absorption coefficients are based on JPL 15-10 (Burkholder et al., 2015). The bromine budget is increased for consistency with observations using additions of $CHBr_3$ and CH_2Br_2, which results in approximately 21 pptv Br_y in the stratosphere around the year 2000. The volume mixing ratio of Cl_y is approximately 3.3 ppbv in the stratosphere over the same period. This nudged CCM is hereafter termed the MIROC-chemical transport model (MIROC-CTM).

3 Method for comparisons between DIAL and MLS/CTM

The O_3 profiles from DIAL are used to evaluate the bias and drift, i.e., long-term stability of satellite measurements (e.g., Nair et al., 2012; Eckert et al., 2014; Hubert et al., 2016). Therefore, it is important to show the quality of the respective ground-

based DIAL performance. Although O_3 profiles at OAPA are included in Hubert et al. (2016), the result for OAPA alone is not shown. Wolfram et al. (2012) also did not show coincident O_3 profiles with any limb-viewing satellite instruments. Therefore, we revisit the quality of the DIAL O_3 profiles obtained in the 2009 austral spring.

Usually, comparisons between DIAL and limb-viewing satellite instruments are conducted considering the differences in their vertical resolution and retrieval strategies (Hubert et al., 2016). MLS has covered the location of OAPA (51.6°S) on a daily basis since measurements began in 2005. The long-term stability of the MLS ozone dataset has been shown to be very good (e.g., Nair et al., 2012; Hubert et al., 2016). As recommended in Livesey et al. (2015), comparisons of MLS with other higher vertical resolution data are achieved by two-step procedure. First, high vertical resolution data, such as those from ozonesondes, should be interpolated with a least squares fit to the profile for each MLS retrieval pressure level, avoiding any layered structures or jagged features, if they exist. The resultant profile is then convolved using the following equation:

$$X_{comv} = X_a + A[X_{DIAL} - X_a] \tag{1}$$

where X_a is the a priori profile for each retrieval and A is the averaging kernel functions (matrix) of MLS. X_{DIAL} is the DIAL ozone profile, and X_{comv} is the convolved DIAL ozone profile, which is converted to each MLS grid for comparison. However, in this study, each DIAL profile was already very smooth, and step one was not necessary. We used A for the polar winter condition from two A that have been provided in the MLS dataset, the other is for the tropical condition.

We used 500 km in distance, the great circle, and ±24 hours for coincidence criteria between DIAL and MLS measurements. Because the mid-point for the DIAL measurement duration was usually 2-3 UTC, the time differences (MLS – DIAL) were 0-4 hours or 13-17 hours on the same day that correspond to night or day paths of the EOS-Aura orbit. When no MLS measurements were available on the same day (9 cases), measurements one day before were used. In those cases, the time differences were –6 to –10 h or –20 to –24 h. For the DIAL measurement on October 27, an MLS measurement on October 28 was used, resulting in a 26 h difference. Both DIAL measurements on October 7 and 8 used ten MLS measurements on October 7 for matching pairs. In total, 180 matching pairs were used in this study.

For comparisons between DIAL and MIROC-CTM, we also unified the vertical grids for comparison. The DIAL profiles were linearly interpolated onto the pressure grids for the MLS data; the vertical increments of the DIAL profile are as small as 150 m. The MIROC-CTM profiles on the day of each DIAL measurement were interpolated onto the pressure grids for the MLS data using a cubic-spline. Both interpolated values were used to compute differences (MIROC-CTM – DIAL) (see Figures 1, 2, and 3).

4 Results and discussion

4.1 Example of vertical profile comparison

Figure 1a shows vertical profiles of O_3 measured with DIAL using Equation (1) compared with those of MLS on the same day (November 14, 2009) as an example. The dotted-line is the original DIAL profile. Each MLS profile was color-scaled with its measurement latitude to observe the latitudinal difference between DIAL and MLS. In addition to the DIAL and MLS

profiles, we also compared the 24 h average O_3 profiles from MIROC-CTM at 12 UTC. Six locations were plotted in Figure 1a (between 48.8°S and 54.4°S in latitude at 67.5°W and 70.3°W in longitude).

On this day, the DIAL profile above 50 hPa, i.e., pressures smaller than that level, revealed lower O_3 values, which was suggested in Wolfram et al. (2012) due to the edge of the southern polar vortex located near OAPA on November 14. Wolfram
5 et al. (2012) also suggested that an altitude region around a potential temperature (PT) of 650 K was just inside the vortex. This DIAL profile agrees well with MLS profiles observed at similar latitudes, 51.7°S with green lines. The MLS profiles revealed a larger latitudinal difference of ~2.5 ppmv over ~8° especially at ~50 hPa level. For reference, the MIROC-CTM profiles also revealed latitudinal differences of ~1 ppmv over 5.6° at the same pressure level, suggesting a weaker latitudinal gradient in the model simulation for these conditions. In addition, the MIROC-CTM O_3 value is higher than from DIAL around 20 hPa
10 levels. We will discuss this feature in the MIROC-CTM in Section 4.2.

In the right panel of Figure 1a, the differences between MLS O_3 and DIAL (MLS – DIAL) are shown. In addition, the difference between DIAL and the nearest MIROC-CTM is shown. In general, the MLS profiles of similar latitudes (51.7°S) with OAPA are in good agreement with the DIAL profile within ±0.5 ppmv between 100 hPa and 6 hPa. The largest negative value is found at 46 hPa, with 2.0 ppmv for a profile of the highest latitude measured (54.7°S). In contrast, the largest positive
15 value is found at 22 hPa, with 1.2 ppmv for a profile of the lowest latitude measured (48.8°S). This indicates that lower O_3 values still exist inside the vortex, i.e., depleted ozone in the spring time has not yet recovered, and larger O_3 values are found outside the vortex at the lower latitudes in the middle stratosphere.

Another example is shown in Figure 1b. On this day, November 23, there were less latitudinal differences in ozone field compared to the result on November 14 as observed by MLS. Consequently, the latitudinal difference in MIROC-CTM is also
20 smaller on November 23 than on November 14. Similar to the former result, the MLS profile at a similar latitude with OAPA is in good agreement with the DIAL profile within ±0.5 ppmv between 83 hPa and 6 hPa. Whereas, the MIROC-CTM O_3 is lower than DIAL by ~−2 ppmv between 10 hPa and 6 hPa.

4.2 Time series comparison

All 23 DIAL profiles obtained in September-November 2009 were evaluated for their variability with time. The PV values at the
25 location and time of all O_3 profiles from DIAL, MLS, and MIROC-CTM were investigated to place the measurements inside or outside the polar vortex. Here, we used meteorological data from the NASA Global Modeling and Assimilation Office (GMAO) Modern-Era Retrospective Analysis for Research and Applications-2 (MERRA-2) reanalysis (Molod et al., 2015; Gelaro et al., 2017) (gmao.gsfc.nasa.gov/reanalysis/MERRA-2/). We calculated the scaled PV (sPV) for pressures between 100 hPa and 6 hPa from the PV values from MERRA-2 and PV/sPV ratios as a function of PT. The PV and sPV values are
30 provided through the MLS website as the derived meteorological products (DMPs) (Manney et al., 2007). We used version 2 of DMP (GEOS5MERRA2 for the version 4 MLS data). sPV values (s^{-1}) are nearly constant at levels throughout the stratosphere (e.g., Dunkerton and Delisi, 1986; Manney et al., 1994, 2007). An sPV value of ~1.4×10^{-4} s^{-1} has been used to define the Northern Hemisphere (N.H.) polar vortex edge center (e.g., Ryan et al., 2016, and references therein). In addition, values of ~1.6 and ~1.2×10^{-4} s^{-1} have been used to define the inner and outer edges, respectively. Those vortex edge definitions,

i.e., center, inner, and outer, are according to Nash et al. (1996). We examined these values using the DMPs for the MLS measurements for the period studied here (i.e., September to November 2009). The results were somewhat different from those from the N.H. depending on time and altitude. For example, center, inner, and outer boundaries are defined by the absolute sPV values of 1.6, 1.9, and 1.3×10^{-4} s^{-1} at 68 hPa in November. The sPV values shown in the following figures are useful
5   guides for showing positions relative to the vortex.

As representatives for the middle and the lower stratospheres, results at 18 hPa and 56 hPa are shown in Figure 2 and Figure 3, respectively. Figure 2a shows the time variation of O$_3$ values obtained from DIAL and MLS at 18 hPa. Both O$_3$ values are color-scaled using sPV values. On several occasions, O$_3$ values below 4 ppmv were measured by DIAL in air masses with larger sPV values, i.e., larger negative values indicated with blue and purple colors, in conjunction with the polar
10   vortex dynamics.

For both September 26 and October 5, the polar vortex shifted toward the South American side, covering the OAPA site. On November 13-14, the O$_3$ values were low again. Correspondingly, the MLS O$_3$ values also show lower values with higher sPV values. In general, the DIAL O$_3$ values are within the variations of MLS O$_3$ values for each coincident date during all comparison periods. To quantitatively evaluate the degree of agreement, the differences between the two (MLS – DIAL) are
15   shown in Figure 2b. These values are color-scaled using the sPV value from each MLS measurement. We computed mean and root-mean-square (rms) differences of O$_3$ from all 180 data points. At 18 hPa, the mean difference is –0.03 ppmv and the rms difference is 0.78 ppmv. Although the mean value shows a good agreement, the variance is large especially in September. We will discuss this large variance in Section 4.3.

Figure 2c for 18 hPa also shows time variations in O$_3$ values obtained from DIAL and those simulated with MIROC-CTM.
20   Figure 2d shows the O$_3$ differences between DIAL and MIROC-CTM (MIROC-CTM – DIAL). In this plot, mean and rms differences in O$_3$ are calculated from all data points of the nearest model grid, 51.6°S/70.3°W, to the OAPA site (the number is 23). As a result, the mean difference is 0.04 ppmv and rms difference is 0.72 ppmv. Similar to the DIAL-MLS comparison, both the DIAL and MIROC-CTM O$_3$ values show low values with larger sPV values, which indicate that the locations are inside the polar vortex, or that the air masses originate from the polar vortex. However, MIROC-CTM overestimates O$_3$ values
25   with the larger sPV values compared to DIAL. When those higher deviations in MIROC-CTM are found, the DIAL O$_3$ values show smaller amounts below ∼4 ppmv (Figure 2c). This is also observed in the vertical profile in Figure 1a. The overestimate of MIROC-CTM may be partly due to the relatively coarse horizontal resolution of the model with regard to a complicated spatial structure near the boundary of the polar vortex in the breakup season. The polar vortex begins to breakup at higher altitudes, and then propagates downward.

30   Figures 3a and 3b show time variations in O$_3$ values from DIAL and MLS, and the difference between the two at 56 hPa, similar to Figures 2a and 2b. Figures 3c and 3d also show time variations in O$_3$ values at 56 hPa from DIAL and MIROC-CTM, and the difference between the two, similar to Figures 2c and 2d. Unlike the characteristics of the 18 hPa result, significant lower ozone values relative to the other dates were not found inside the polar vortex on September 26 and October 5. Whereas, on November 13-14 and 23-24, lower O$_3$ values inside the polar vortex were found from both of DIAL and MLS. This is in
35   agreement with the long-lasting polar vortex dynamics in the 2009 spring (de Laat et al., 2010; Wolfram et al., 2012). The mean

differences between DIAL and MLS/MIROC-CTM are as small as 0.06 ppmv and 0.16 ppmv, respectively. The rms differences are 0.46 ppmv and 0.36 ppmv for DIAL/MLS and DIAL/MIROC-CTM comparisons, respectively, which are smaller values than those at 18 hPa. The overestimate of MIROC-CTM with larger sPV values, as seen at 18 hPa is not evident at 56 hPa. One explanation may be that the polar vortex is more stable at 56 hPa than at 18 hPa, even on November 23-24.

5   ## 4.3   Dependency in distance and sPV difference

The good correlation between sPV and O_3 values near the vortex boundary in austral spring has been previously shown in satellite measurements (e.g., Manney et al., 1999, 2001, 2005). Therefore, a horizontal gradient in O_3 should have been present at the vortex boundary in the 2009 spring. A previous study suggested that a better agreement is found when the comparison is performed with matching meteorological conditions using parameters such as sPV and equivalent latitude (Manney et al.,

10   2001). Therefore, we further examined the larger variability between DIAL and MLS at 18 hPa, from the perspective of different sPV values. Figure 4a shows the O_3 difference (MLS – DIAL) versus sPV difference between DIAL and MLS (MLS – DIAL). Similar to Figure 2b, the data points are color-scaled based on the sPV values of the MLS measurements. A positive correlation between O_3 and sPV differences is found, suggesting lower O_3 values in MLS (negative in the y-axis) with a more poleward MLS profile, i.e., negative in the x-axis. Conversely, higher O_3 values in MLS, i.e., positive in the y-axis, with the

15   lower latitude side profile in MLS, i.e., positive in the x-axis, is also seen, although the correlation is weaker than in the negative value area. After filtering out matching pairs over a certain sPV difference, e.g., below or above $\pm 0.3 \times 10^{-4}$ s^{-1}, the rms difference between DIAL and MLS at this pressure level decreases significantly. Such an sPV criterion is useful for suppressing the large rms difference found in O_3 measurements affected by the motion of polar vortex. Whereas, the mean difference less changes applying such the sPV criterion. This is consistent with the result from Holl et al. (2016) who showed differences in

20   CH_4 values observed in the northern high latitude and sPV criterion with a value of 0.2×10^{-4} s^{-1} has little effect below 25 km in altitude.

We also examined results from 56 hPa in Figure 4b. Similar to the results from 18 hPa, larger O_3 differences are found with larger sPV differences. Applying certain sPV criterion to these data, the mean difference changes only slightly, but the rms difference decreases, similar to the results from 18 hPa. The results for other pressure levels are summarized in Section 4.4.

25   In addition to the sPV differences examined, we evaluated the correlation between the O_3 difference and distance in the DIAL/MLS measurements (Figure 5). In these figures (Figure 5a for 18 hPa and Figure 5b for 56 hPa), data points are color-scaled based on the sPV difference between DIAL and MLS (MLS – DIAL). Clearly, larger O_3 differences, especially those with negative values in Figure 5a, have large sPV differences, i.e., below -0.5×10^{-4} s^{-1}). As shown in the figures, the O_3 difference does not depend critically on the distance between the two measurements.

30   In summary, the O_3 differences between DIAL and MLS can be partly attributed to differences in the measurement points. Furthermore, the O_3 difference is more correlated with sPV differences between than the difference in distance. Therefore, it is important to analyze O_3 values with sPV (or PV) values near the polar vortex boundary, which has been suggested previously (e.g., Manney et al., 2001).

4.4 Comparison at other levels: summary

The mean and rms differences computed from the time-series comparisons in Section 4.2 were extended for other pressure
levels to summarize the degree of agreement between DIAL and MLS or MIROC-CTM. These results are plotted versus
pressure in Figure 6. Absolute differences are shown in the left panel. Relative differences, the absolute differences divided

5   by their mean values of O_3, are shown in the right panel. In the left panel, mean differences (open circle and cross) for both
DIAL/MLS and DIAL/MIROC-CTM comparisons, along with rms differences (dotted lines) are shown. The mean differences
of the DIAL/MLS comparison are almost within ± 0.1 ppmv between 6 hPa and 56 hPa with 180 data points for each level.
This corresponds to the relative values, in the right panel, of $\pm 3\%$. Figure 7 shows differences between DIAL and MLS using
the sPV criterion. The mean and rms differences shown in this figure as blue lines are identical to Figure 6. The mean and

10   rms differences after filtering with the sPV criteria ($\pm 0.3 \times 10^{-4}$ s^{-1}) are shown as green lines. Clearly, the rms differences
decrease 21-47% between 10 hPa and 56 hPa; the number of data points was reduced from 146-180 to 107-144. However, the
mean differences only change slightly for all pressure levels, except for the 6 hPa level.

    For the DIAL/MIROC-CTM comparison, the mean differences are almost within ± 0.3 ppmv between 10 hPa and 56 hPa,
with 23 data points for each level. This corresponds to relative values of $\pm 8\%$. Above 8 hPa, the absolute differences increase to

15   –0.6 ppmv which corresponds to relative values of –8%. Although not shown in the figure, a time-series for 6-8 hPa shows that
larger negative deviations in MIROC-CTM are observed in October and November. The peak altitude of ozone in MIROC-CTM
is lower than that of DIAL, as shown in Figure 1. Both the vertical and horizontal motions of air in the model are responsible
for this different feature, but the cause is not known. The feature presented here suggests a difficulty in the reproduced ozone
field for those pressure levels (6-8 hPa) in these latitudes and season using this version of MIROC-CTM. As discussed in

20   Section 4.2, the polar vortex breakup process may cause a highly variable spatial structure. This may be partly responsible for
the difference because of the insufficient spatial resolution of the model to distinguish this process.

    Both the DIAL/MLS and DIAL/MIROC-CTM comparisons show increasing rms differences with increasing altitudes above
the 20-30 hPa levels, reaching more than 1 ppmv. This is partly due to the O_3 value increasing with increasing altitudes.
Thus, relative values of the rms difference (Figure 6b) do not show strong vertical gradients compared to the absolute values

25   (Figure 6a).

    Both comparisons also show larger absolute differences below 68 hPa, reaching 0.5 ppmv (73%) for DIAL/MLS and 0.9
ppmv (119%) for DIAL/MIROC-CTM. This suggests a lower bias in the DIAL measurement at these lower altitudes ($\sim$80-100
hPa) of some magnitude. As discussed in Wolfram et al. (2008), this DIAL system has some difficulty in measuring around 100
hPa and below due to saturation from backscattered photons in the low-energy channels. Therefore, DIAL data at this altitude

30   range should be used with caution.

    Another possible reason is the difference in measured ozone associated with the difference in original vertical resolution,
$\sim$1 km for DIAL versus 3 km for MLS. In this period, lamina structures in O_3 profiles are often observed from ozonesonde
measurements, especially below 20 km. DIAL may capture lower values of O_3 in these lamina structures while collecting
measurements over 3-5 h, compared to MLS that measures instantaneously along the orbit, nearly the north-south direction

(see Supplement). This may facilitate O_3 differences, to a certain extent, even while both measurements are accurate. In the other geophysical regions of the Asian monsoon anticyclone, difficulties in MLS retrievals within the strong vertical gradient of O_3 have been discussed (Yan et al., 2016). The largest O_3 difference between DIAL and MLS at 83 hPa was found on October 3, 2009; this case was studied using air mass trajectory analysis (Tomikawa and Sato, 2005) and the O_3 field from
5 MIROC-CTM (see Supplement).

5 Conclusions

Ground-based DIAL measurements were performed at the OAPA in Río Gallegos (51.6°S, 69.3°W), Argentina, from September to November 2009, when a long-lasting southern polar vortex, and accompanying ozone depletion, occurred over the area for the first time since 1979 (de Laat et al., 2010; Wolfram et al., 2012). This site is one of the few NDACC DIAL sites in the
10 S.H. Focusing on this period of large dynamical variability in measured air masses during the movement of the polar vortex, it is possible to analyze the effects of the polar vortex on O_3 variability. Twenty-three O_3 profiles were obtained by DIAL during the period. These profiles were compared with coincident MLS O_3 profiles with 180 matching pairs, based on time and space criteria.

The mean differences between DIAL and MLS are within ±0.1 ppmv (±3%) from 6 hPa to 56 hPa, showing good agreement
15 regardless of the large sPV variability between each matching pair. The DIAL data are also compared with outputs from the MIROC-CTM model simulation. The mean differences between DIAL and MIROC-CTM are within ±0.3 ppmv (±8%) from 10 hPa to 56 hPa. Above 8 hPa, the mean differences increases to –0.6 ppmv (–8%). To measure variability in the comparison, rms differences between DIAL and MLS or MIROC-CTM are also evaluated. For both DIAL/MLS and DIAL/MIROC-CTM comparisons, the rms differences are nearly 0.5 ppmv for pressure levels between 30 hPa and 100 hPa, and increase with
20 increasing altitudes up to 6 hPa, reaching 1.1-1.2 ppmv. From the DIAL/MLS comparison, the O_3 differences depend on sPV differences at 18 hPa. Therefore, another criterion for comparison is proposed: pairs with absolute sPV differences that exceed $0.3 \times 10^{-4}\,\mathrm{s}^{-1}$ are discarded. As a result, the rms differences decreased significantly between 10 hPa and 56 hPa, but the mean differences only slightly change for all pressure levels, except for 6 hPa.

The comparison between DIAL and MLS indicates that the O_3 difference is partly due to sPV differences between measure-
25 ment locations; however as yet unknown factors create additional differences. The comparison between DIAL and MIROC-CTM indicates that an insufficient model spatial resolution may be partly responsible for the O_3 differences above 18 hPa during polar vortex breakup. Both the DIAL/MLS and DIAL/MIROC-CTM comparisons also show larger mean differences below 68 hPa, reaching 0.5 ppmv (73%) and 0.9 ppmv (119%) at 100 hPa, respectively. One possible cause may be a low bias in the DIAL O_3 measurement, but this hypothesis was not confirmed in this study. Nevertheless, finding good agreement
30 between DIAL and MLS O_3 measurements between 6 hPa and 56 hPa is a necessary step for studies in evaluating bias and long-term stability of satellite sensors in the future. This study provides an outlook for continuing measurements at the OAPA site. The DIAL measurements at the OAPA site are available for all years since 2005, except 2016 when no measurements were collected. The result of the DIAL/MLS comparison using these long-term data will be published elsewhere.

Acknowledgements. This research was supported by the Science and Technology Research Partnership for Sustainable Development (SATREPS), Japan Science and Technology Agency (JST) and Japan International Cooperation Agency (JICA). The DIAL construction and maintenance from 2005 until the present were supported by projects lead by Eduardo Quel (CEILAP), type PICT from the Science and Technology Ministry of Argentine, and in collaboration with CONICET, and the late Gérard Mégie and Sophie Godin-Beekmann (CNRS, France), and Hideaki Nakane (Kochi University of Technology, Japan). The Aura MLS data were produced at the Jet Propulsion Laboratory (JPL), California Institute of Technology, under contract with the National Aeronautics and Space Administration (NASA). CTM computations were conducted on NEC-SX9/A(ECO) computers at CGER, NIES. We thank Yousuke Yamashita (Japan Agency for Marine-Earth Science and Technology), and Haruna Nakamura and Izumi Ikeuchi (Fujitsu FIP Corp., Japan) for configuring and preparing the model computations. The derived meteorological products (DMPs) were produced by Gloria L. Manney (NorthWest Research Associates and New Mexico Institute of Mining and Technology) and Luis F. Millán (NASA/JPL). We thank Masanao Kadowaki (Japan Atomic Energy Agency) for his helpful discussion in the early stages of this manuscript. The air mass trajectories were computed by the National Institute of Polar Research, Japan, trajectory model using the NASA GMAO's MERRA data. We would like to thank Editage (www.editage.jp) for English language editing.

References

Akiyoshi, H., Nakamura, T., Miyasaka, T., Shiotani, M., and Suzuki, M.: A nudged chemistry-climate model simulation of chemical con-
stituent distribution at northern high-latitude stratosphere observed by SMILES and MLS during the 2009/2010 stratospheric sudden
warming, J. Geophy. Res., 121, 1361–1380, https://doi.org/10.1002/2015JD023334, http://dx.doi.org/10.1002/2015JD023334, 2016.

5 Antuña-Marrero, J. C., Landulfo, E., Estevan, R., Barja, B., Robock, A., Wolfram, E., Ristori, P., Clemesha, B., Zaratti, F., Forno, R.,
Armandillo, E., Bastidas, A. E., de Frutos Baraja, A. M., Whiteman, D. N., Quel, E., Barbosa, H. M. J., Lopes, F., Montilla-Rosero, E.,
and Guerrero-Rascado, J. L.: LALINET: The First Latin American-born Regional Atmospheric Observational Network, Bull. American
Meteorol. Soc., 98, 1255–1275, https://doi.org/10.1175/BAMS-D-15-00228.1, https://doi.org/10.1175/BAMS-D-15-00228.1, 2017.

Burkholder, J. B., Sander, S. P., Abbatt, J., Barker, J. R., Huie, R. E., Kolb, C. E., Kurylo, M. J., Orkin, V. L., Wilmouth, D. M., and
10 Wine, P. H.: Chemical Kinetics and Photochemical Data for Use in Atmospheric Studies, Evaluation No. 18, JPL Publication 15-10, Jet
Propulsion Laboratory, Pasadena, http://jpldataeval.jpl.nasa.gov, 2015.

CIRA: COSPAR International Reference Atmosphere 1986, Part II: Middle Atmosphere Models, Adv. Space Res., Vol. 10, No. 12, Pergamon
Press, Oxford and NY, pp. 519, 1990.

de Laat, A. T. J., van der A, R. J., Allaart, M. A. F., van Weele, M., Benitez, G. C., Casiccia, C., Paes Leme, N. M., Quel, E., Salvador, J., and
15 Wolfram, E.: Extreme sunbathing: Three weeks of small total O_3 columns and high UV radiation over the southern tip of South America
during the 2009 Antarctic O_3 hole season, Geophys. Res. Lett., 37, L14 805, https://doi.org/10.1029/2010GL043699, 2010.

Dee, D. P., Uppala, S. M., Simmons, A. J., Berrisford, P., Poli, P., Kobayashi, S., Andrae, U., Balmaseda, M. A., Balsamo, G., Bauer, P.,
Bechtold, P., Beljaars, A. C. M., van de Berg, L., Bidlot, J., Bormann, N., Delsol, C., Dragani, R., Fuentes, M., Geer, A. J., Haimberger,
L., Healy, S. B., Hersbach, H., Hólm, E. V., Isaksen, L., Kållberg, P., Köhler, M., Matricardi, M., McNally, A. P., Monge-Sanz, B. M.,
20 Morcrette, J.-J., Park, B., Peubey, C., de Rosnay, P., Tavolato, C., Thépaut, J.-N., and Vitart, F.: The ERA-Interim reanalysis: configuration
and performance of the data assimilation system, Q. J. Roy. Meteor. Soc., 137, 553–597, https://doi.org/10.1002/qj.828, http://dx.doi.org/
10.1002/qj.828, 2011.

Dunkerton, T. J. and Delisi, D. P.: Evolution of potential vorticity in the winter stratosphere of January-February 1979, J. Geophys. Res., 91,
1199–1208, https://doi.org/10.1029/JD091iD01p01199, http://dx.doi.org/10.1029/JD091iD01p01199, 1986.

25 Eckert, E., von Clarmann, T., Kiefer, M., Stiller, G. P., Lossow, S., Glatthor, N., Degenstein, D. A., Froidevaux, L., Godin-Beekmann, S.,
Leblanc, T., McDermid, S., Pastel, M., Steinbrecht, W., Swart, D. P. J., Walker, K. A., and Bernath, P. F.: Drift-corrected trends and
periodic variations in MIPAS IMK/IAA ozone measurements, Atmos. Chem. Phys., 14, 2571–2589, https://doi.org/10.5194/acp-14-2571-
2014, http://www.atmos-chem-phys.net/14/2571/2014/, 2014.

Gelaro, R., McCarty, W., Suárez, M. J., Todling, R., Molod, A., Takacs, L., Randles, C. A., Darmenov, A., Bosilovich, M. G., Reichle,
30 R., Wargan, K., Coy, L., Cullather, R., Draper, C., Akella, S., Buchard, V., Conaty, A., da Silva, A. M., Gu, W., Kim, G.-K., Koster,
R., Lucchesi, R., Merkova, D., Nielsen, J. E., Partyka, G., Pawson, S., Putman, W., Rienecker, M., Schubert, S. D., Sienkiewicz, M.,
and Zhao, B.: The Modern-Era Retrospective Analysis for Research and Applications, Version 2 (MERRA-2), J. Clim., 30, 5419–5454,
https://doi.org/10.1175/JCLI-D-16-0758.1, https://doi.org/10.1175/JCLI-D-16-0758.1, 2017.

Godin, S., Mégie, G., and Pelon, J.: Systematic lidar measurements of the stratospheric ozone vertical distribution, Geophys. Res. Lett., 16,
35 547–550, https://doi.org/10.1029/GL016i006p00547, http://dx.doi.org/10.1029/GL016i006p00547, 1989.

Holl, G., Walker, K. A., Conway, S., Saitoh, N., Boone, C. D., Strong, K., and Drummond, J. R.: Methane cross-validation between three
Fourier transform spectrometers: SCISAT ACE-FTS, GOSAT TANSO-FTS, and ground-based FTS measurements in the Canadian high

Arctic, Atmos. Meas. Tech., 9, 1961–1980, https://doi.org/10.5194/amt-9-1961-2016, http://www.atmos-meas-tech.net/9/1961/2016/, 2016.

Hubert, D., Lambert, J.-C., Verhoelst, T., Granville, J., Keppens, A., Baray, J.-L., Bourassa, A. E., Cortesi, U., Degenstein, D. A., Froidevaux, L., Godin-Beekmann, S., Hoppel, K. W., Johnson, B. J., Kyrölä, E., Leblanc, T., Lichtenberg, G., Marchand, M., McElroy, C. T., Murtagh, D., Nakane, H., Portafaix, T., Querel, R., Russell III, J. M., Salvador, J., Smit, H. G. J., Stebel, K., Steinbrecht, W., Strawbridge, K. B., Stübi, R., Swart, D. P. J., Taha, G., Tarasick, D. W., Thompson, A. M., Urban, J., van Gijsel, J. A. E., Van Malderen, R., von der Gathen, P., Walker, K. A., Wolfram, E., and Zawodny, J. M.: Ground-based assessment of the bias and long-term stability of 14 limb and occultation ozone profile data records, Atmos. Meas. Tech., 9, 2497–2534, https://doi.org/10.5194/amt-9-2497-2016, http://www.atmos-meas-tech.net/9/2497/2016/, 2016.

Jiang, Y. B., Froidevaux, L., Lambert, A., Livesey, N. J., Read, W. G., Waters, J. W., Bojkov, B., Leblanc, T., McDermid, I. S., Godin-Beekmann, S., Filipiak, M. J., Harwood, R. S., Fuller, R. A., Daffer, W. H., Drouin, B. J., Cofield, R. E., Cuddy, D. T., Jarnot, R. F., Knosp, B. W., Perun, V. S., Schwartz, M. J., Snyder, W. V., Stek, P. C., Thurstans, R. P., Wagner, P. A., Allaart, M., Andersen, S. B., Bodeker, G., Calpini, B., Claude, H., Coetzee, G., Davies, J., De Backer, H., Dier, H., Fujiwara, M., Johnson, B., Kelder, H., Leme, N. P., König-Langlo, G., Kyro, E., Laneve, G., Fook, L. S., Merrill, J., Morris, G., Newchurch, M., Oltmans, S., Parrondos, M. C., Posny, F., Schmidlin, F., Skrivankova, P., Stubi, R., Tarasick, D., Thompson, A., Thouret, V., Viatte, P., Vömel, H., von der Gathen, P., Yela, M., and Zablocki, G.: Validation of Aura Microwave Limb Sounder Ozone by ozonesonde and lidar measurements, J. Geophys. Res., 112, https://doi.org/10.1029/2007JD008776, http://dx.doi.org/10.1029/2007JD008776, 2007.

Livesey, N. J., Santee, M. L., and Manney, G. L.: A Match-based approach to the estimation of polar stratospheric ozone loss using Aura Microwave Limb Sounder observations, Atmospheric Chemistry and Physics, 15, 9945–9963, https://doi.org/10.5194/acp-15-9945-2015, http://www.atmos-chem-phys.net/15/9945/2015/, 2015.

Manney, G. L., Zurek, R. W., O'Neill, A., and Swinbank, R.: On the Motion of Air through the Stratospheric Polar Vortex, J. Atmos. Sci., 51, 2973–2994, https://doi.org/10.1175/1520-0469(1994)051<2973:OTMOAT>2.0.CO;2, http://dx.doi.org/10.1175/1520-0469(1994)051<2973:OTMOAT>2.0.CO;2, 1994.

Manney, G. L., Michelsen, H. A., Santee, M. L., Gunson, M. R., Irion, F. W., Roche, A. E., and Livesey, N. J.: Polar vortex dynamics during spring and fall diagnosed using trace gas observations from the Atmospheric Trace Molecule Spectroscopy instrument, J. Geophys. Res., 104, 18 841–18 866, https://doi.org/10.1029/1999JD900317, http://dx.doi.org/10.1029/1999JD900317, 1999.

Manney, G. L., Michelsen, H. A., Bevilacqua, R. M., Gunson, M. R., Irion, F. W., Livesey, N. J., Oberheide, J., Riese, M., Russell, J. M., Toon, G. C., and Zawodny, J. M.: Comparison of satellite ozone observations in coincident air masses in early November 1994, J. Geophys. Res., 106, 9923–9943, https://doi.org/10.1029/2000JD900826, http://dx.doi.org/10.1029/2000JD900826, 2001.

Manney, G. L., Santee, M. L., Livesey, N. J., Froidevaux, L., Read, W. G., Pumphrey, H. C., Waters, J. W., and Pawson, S.: EOS Microwave Limb Sounder observations of the Antarctic polar vortex breakup in 2004, Geophys. Res. Lett., 32, https://doi.org/10.1029/2005GL022823, http://dx.doi.org/10.1029/2005GL022823, 2005.

Manney, G. L., Daffer, W. H., Zawodny, J. M., Bernath, P. F., Hoppel, K. W., Walker, K. A., Knosp, B. W., Boone, C., Remsberg, E. E., Santee, M. L., Harvey, V. L., Pawson, S., Jackson, D. R., Deaver, L., McElroy, C. T., McLinden, C. A., Drummond, J. R., Pumphrey, H. C., Lambert, A., Schwartz, M. J., Froidevaux, L., McLeod, S., Takacs, L. L., Suarez, M. J., Trepte, C. R., Cuddy, D. C., Livesey, N. J., Harwood, R. S., and Waters, J. W.: Solar occultation satellite data and derived meteorological products: Sampling issues and comparisons with Aura Microwave Limb Sounder, J. Geophys. Res., 112, D24S50, https://doi.org/10.1029/2007JD008709, 2007.

Molod, A., Takacs, L., Suarez, M., and Bacmeister, J.: Development of the GEOS-5 atmospheric general circulation model: evolution from MERRA to MERRA2, Geosci. Model Dev., 8, 1339–1356, https://doi.org/10.5194/gmd-8-1339-2015, http://www.geosci-model-dev.net/8/1339/2015/, 2015.

Nair, P. J., Godin-Beekmann, S., Pazmiño, A., Hauchecorne, A., Ancellet, G., Petropavlovskikh, I., Flynn, L. E., and Froidevaux, L.: Coherence of long-term stratospheric ozone vertical distribution time series used for the study of ozone recovery at a northern mid-latitude station, Atmos. Chem. Phys., 11, 4957–4975, https://doi.org/10.5194/acp-11-4957-2011, http://www.atmos-chem-phys.net/11/4957/2011/, 2011.

Nair, P. J., Godin-Beekmann, S., Froidevaux, L., Flynn, L. E., Zawodny, J. M., Russell III, J. M., Pazmiño, A., Ancellet, G., Steinbrecht, W., Claude, H., Leblanc, T., McDermid, S., van Gijsel, J. A. E., Johnson, B., Thomas, A., Hubert, D., Lambert, J.-C., Nakane, H., and Swart, D. P. J.: Relative drifts and stability of satellite and ground-based stratospheric ozone profiles at NDACC lidar stations, Atmos. Meas. Tech., 5, 1301–1318, https://doi.org/10.5194/amt-5-1301-2012, http://www.atmos-meas-tech.net/5/1301/2012/, 2012.

Nash, E. R., Newman, P. A., Rosenfield, J. E., and Schoeberl, M. R.: An objective determination of the polar vortex using Ertel's potential vorticity, J. Geophys. Res., 101, 9471–9478, https://doi.org/10.1029/96JD00066, http://dx.doi.org/10.1029/96JD00066, 1996.

Ryan, N. J., Walker, K. A., Raffalski, U., Kivi, R., Gross, J., and Manney, G. L.: Ozone profiles above Kiruna from two ground-based radiometers, Atmos. Meas. Tech., 9, 4503–4519, https://doi.org/10.5194/amt-9-4503-2016, http://www.atmos-meas-tech.net/9/4503/2016/, 2016.

Steinbrecht, W., Froidevaux, L., Fuller, R., Wang, R., Anderson, J., Roth, C., Bourassa, A., Degenstein, D., Damadeo, R., Zawodny, J., Frith, S., McPeters, R., Bhartia, P., Wild, J., Long, C., Davis, S., Rosenlof, K., Sofieva, V., Walker, K., Rahpoe, N., Rozanov, A., Weber, M., Laeng, A., von Clarmann, T., Stiller, G., Kramarova, N., Godin-Beekmann, S., Leblanc, T., Querel, R., Swart, D., Boyd, I., Hocke, K., Kämpfer, N., Maillard Barras, E., Moreira, L., Nedoluha, G., Vigouroux, C., Blumenstock, T., Schneider, M., Garcìa, O., Jones, N., Mahieu, E., Smale, D., Kotkamp, M., Robinson, J., Petropavlovskikh, I., Harris, N., Hassler, B., Hubert, D., and Tummon, F.: An update on ozone profile trends for the period 2000 to 2016, Atmos. Chem. Phys. Discuss., 2017, 1–24, https://doi.org/10.5194/acp-2017-391, http://www.atmos-chem-phys-discuss.net/acp-2017-391/, 2017.

Tomikawa, Y. and Sato, K.: Design of NIPR trajectory model, Polar Meteorol. Glaciol., 19, 120–137, http://ci.nii.ac.jp/naid/110002261737/en/, 2005.

Waters, J., Froidevaux, L., Harwood, R., Jarnot, R., Pickett, H., Read, W., Siegel, P., Cofield, R., Filipiak, M., Flower, D., Holden, J., Lau, G., Livesey, N., Manney, G., Pumphrey, H., Santee, M., Wu, D., Cuddy, D., Lay, R., Loo, M., Perun, V., Schwartz, M., Stek, P., Thurstans, R., Boyles, M., Chandra, K., Chavez, M., Chen, G.-S., Chudasama, B., Dodge, R., Fuller, R., Girard, M., Jiang, J., Jiang, Y., Knosp, B., LaBelle, R., Lam, J., Lee, K., Miller, D., Oswald, J., Patel, N., Pukala, D., Quintero, O., Scaff, D., Van Snyder, W., Tope, M., Wagner, P., and Walch, M.: The Earth Observing System Microwave Limb Sounder (EOS MLS) on the Aura satellite, Geoscience and Remote Sensing, IEEE Transactions on, 44, 1075–1092, https://doi.org/10.1109/TGRS.2006.873771, 2006.

WMO: Scientific Assessment of Ozone Depletion: 2014, Global Ozone Research and Monitoring Project–Report No. 55, 516 pp., Geneva, Switzerland, 2014.

Wolfram, E. A., Salvador, J., D'Elia, R., Casiccia, C., Leme, N. P., Pazmiño, A., Porteneuve, J., Godin-Beekman, S., Nakane, H., and Quel, E. J.: New differential absorption lidar for stratospheric ozone monitoring in Patagonia, South Argentina, J. Opt. A: Pure Appl. Opt., 10, 104 021, http://stacks.iop.org/1464-4258/10/i=10/a=104021, 2008.

Wolfram, E. A., Salvador, J., Orte, F., D'Elia, R., Godin-Beekmann, S., Kuttippurath, J., Pazmiño, A., Goutail, F., Casiccia, C., Zamorano, F., Paes Leme, N., and Quel, E. J.: The unusual persistence of an ozone hole over a southern mid-latitude station during the Antarctic spring

2009: a multi-instrument study, Ann. Geophys., 30, 1435–1449, https://doi.org/10.5194/angeo-30-1435-2012, http://www.ann-geophys.net/30/1435/2012/, 2012.

Yan, X., Wright, J. S., Zheng, X., Livesey, N. J., Vömel, H., and Zhou, X.: Validation of Aura MLS retrievals of temperature, water vapour and ozone in the upper troposphere and lower–middle stratosphere over the Tibetan Plateau during boreal summer, Atmos. Meas. Tech.,

5   9, 3547–3566, https://doi.org/10.5194/amt-9-3547-2016, http://www.atmos-meas-tech.net/9/3547/2016/, 2016.
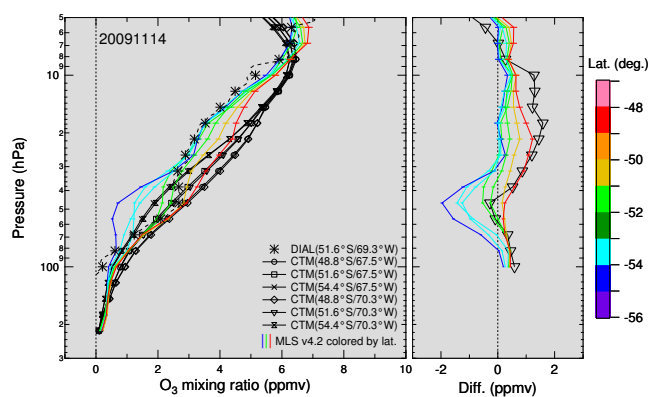
(a)
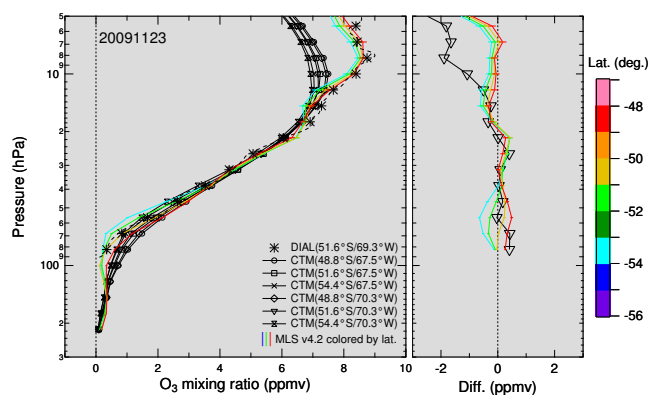
(b)

Figure 1. Vertical profiles of O₃ mixing ratios on November 14, 2009 (a) and November 23, 2009 (b) measured using DIAL (plus-crosses and dotted-line) and MLS (solid-lines with color) over the OAPA site (see text for additional description). MIROC-CTM O₃ profiles around the OAPA site are also shown for six grids. Differences between DIAL and X (MLS or MIROC-CTM) (X – DIAL) are shown in the right panel (see text). The MLS profiles are color-scaled based on their measurement latitudes.
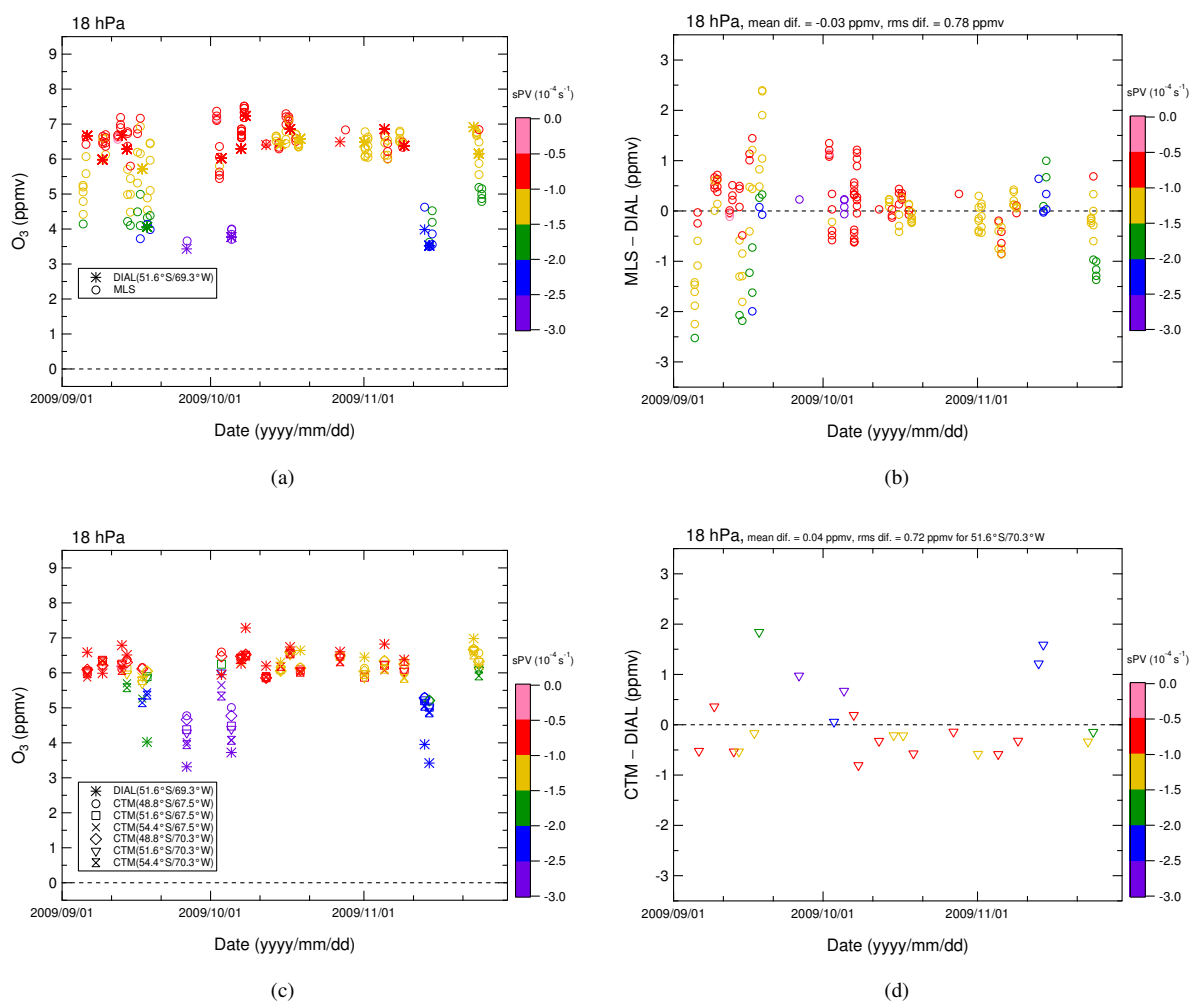
Figure 2. Time series of O_3 mixing ratios as measured by DIAL and MLS at 18 hPa (a) and differences between the two (b) from September to November 2009, over the OAPA site. (c) and (d) are same as (a) and (b), but for DIAL and MIROC-CTM. Data are color-scaled based on sPV values.
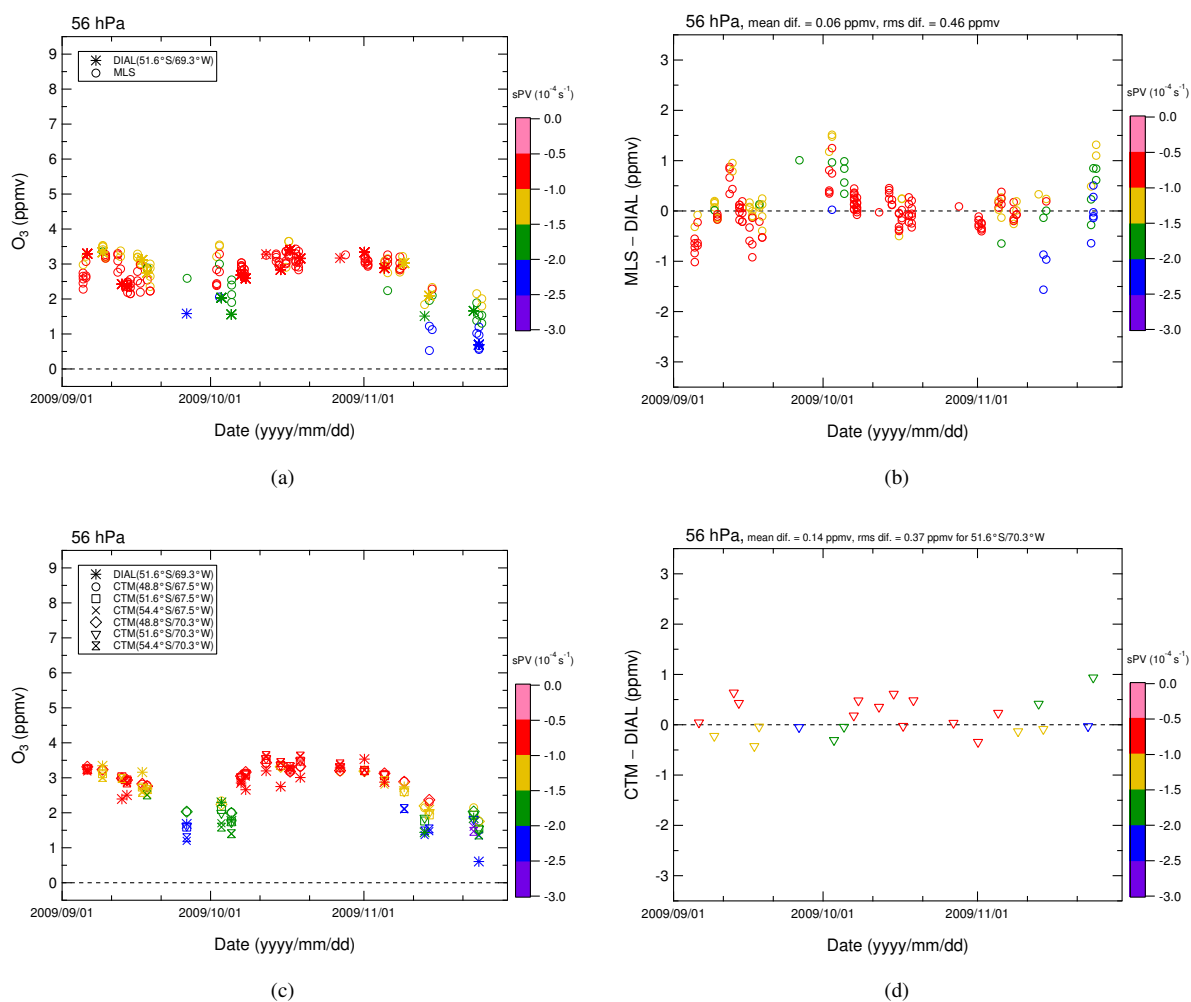
Figure 3. Time series of O$_3$ mixing ratios as measured by DIAL and MLS at 56 hPa (a) and differences between the two (b) from September to November 2009, over the OAPA site. (c) and (d) are same as (a) and (b), but for DIAL and MIROC-CTM. Data are color-scaled based on sPV values.
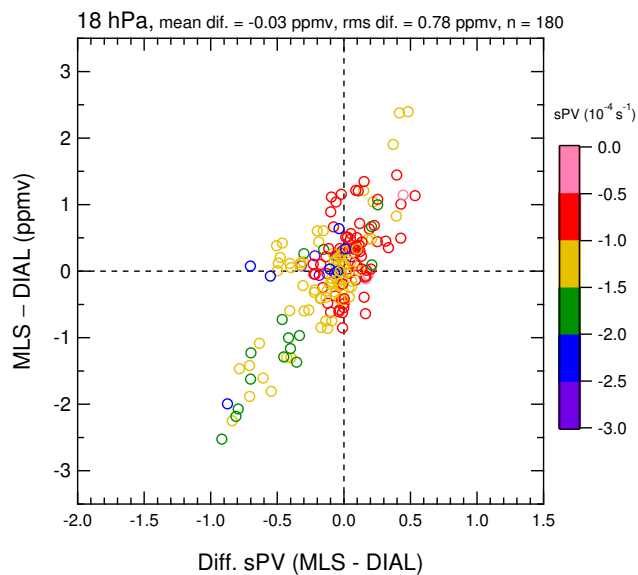
(a)
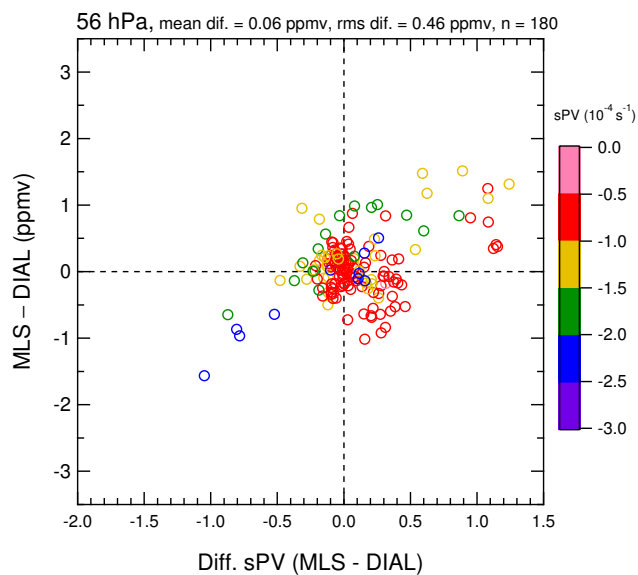
(b)

Figure 4. O_3 difference versus sPV difference for DIAL and MLS at 18 hPa (a) and 56 hPa (b). Data are color-scaled based on the sPV for the MLS measurements.
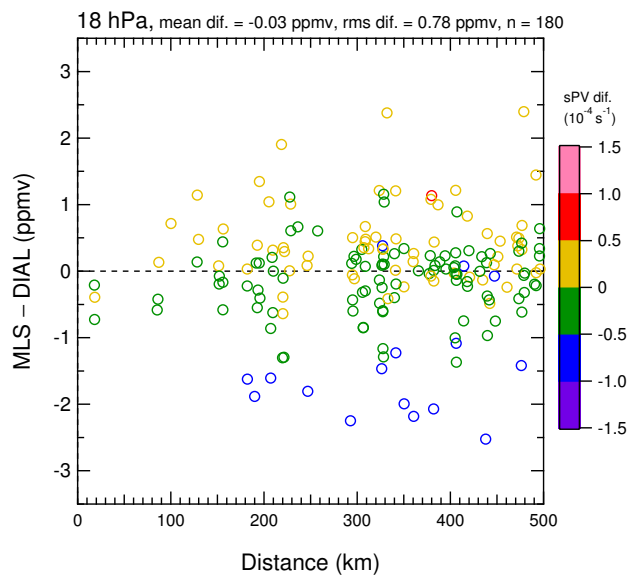
(a)
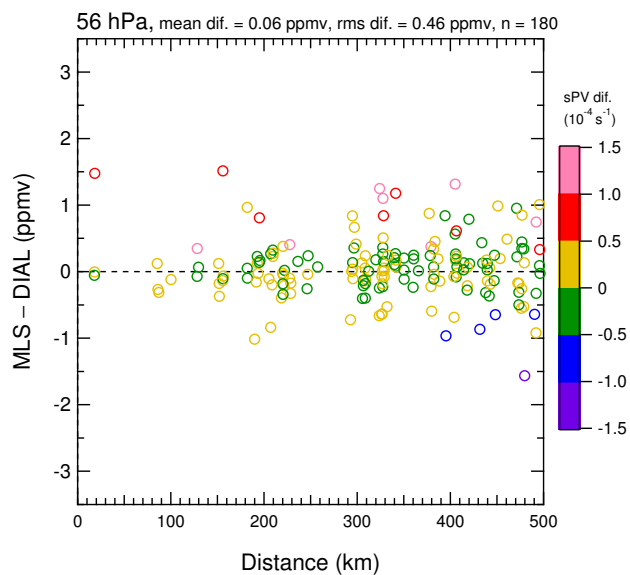
(b)

Figure 5. O_3 difference versus distance for DIAL and MLS at 18 hPa (a) and 56 hPa (b). Data are color-scaled based on sPV differences between DIAL and MLS measurements.

(a)   (b)
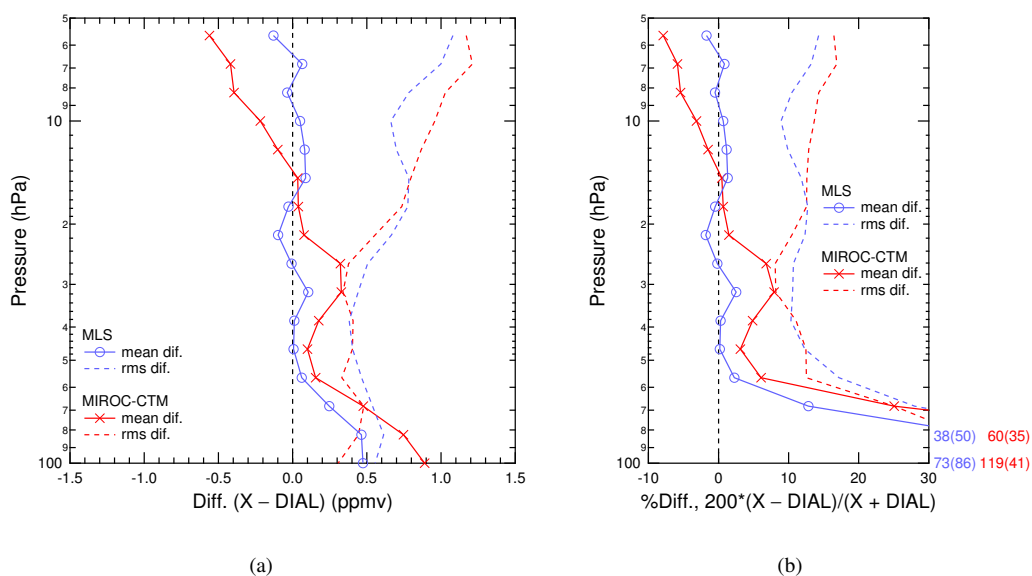
Figure 6. Vertical profiles of mean and rms differences of O$_3$ values for DIAL and X (MLS or MIROC-CTM) (a) and those of relative values (b). Each value is computed from each pressure level in the time series as shown in Figures 2 and 3. The numbers outside the plot are values of the mean (rms in parentheses) difference at 83 hPa and 100 hPa.
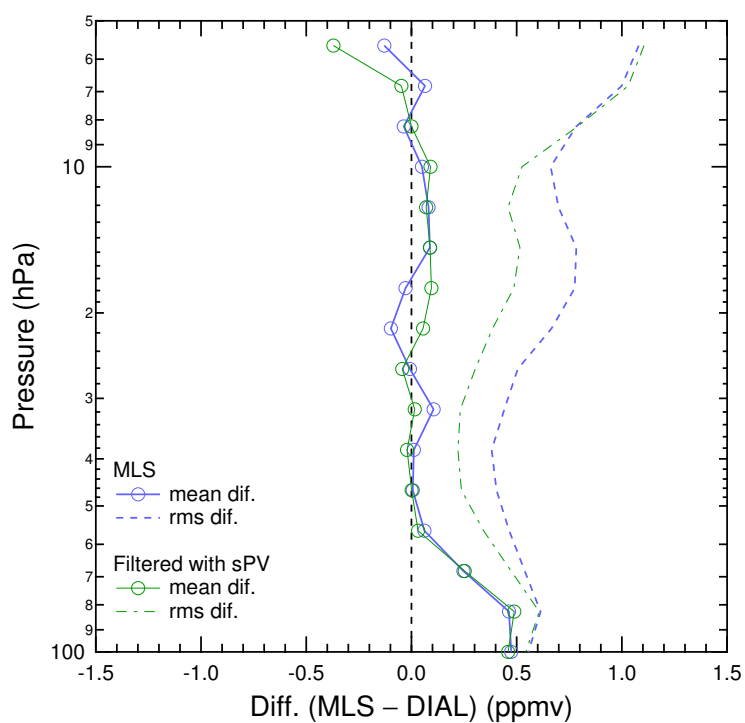
Figure 7. Vertical profiles of mean and rms differences with and without scaled PV criterion screening for the DIAL/MLS O_3 comparison.